Electronic Supplementary Information

Metal-Organic Cage Incorporating Thin-Film Nanocomposite Membranes with Antifouling Properties

*Yi Di Yuan, Xiaomei Zhang,† Ziqi Yang and Dan Zhao**

Department of Chemical & Biomolecular Engineering, National University of Singapore, 117585 Singapore

†Institute of Agricultural Facilities and Equipment, Jiangsu Academy of Agricultural Sciences, Nanjing 210014, China

Materials and Methods

Materials and Chemicals. All chemicals were obtained from commercial suppliers and used without further purification. Polyethersulfone (PES) ultrafiltration (UF) membrane (UE005, RisingSun Membrane, Beijing, China) was used as the backing substrate to prepare thin-film nanocomposite membranes. m-Phenylenediamine (MPD, > 99%), trimesoyl chloride (TMC, 98%), titanium (IV) chloride ($TiCl_4$, 1.0 M in toluene), titanium (IV) oxide (Aeroxide, nanopowder, 21 nm primary particle size (TEM), ≥ 99.5% trace metals basis), bovine serum albumin (BSA), and albumin-fluorescein isothiocyanate conjugate (BSA-FITC) were obtained from Sigma-Aldrich. Zirconocene dichloride (Cp_2ZrCl_2, > 99%) and pamoic acid (97%) were obtained from Aladdin. Dodecyltrimethylammonium bromide (DTAB, > 98%) and 2-aminoterephthalic acid (> 98%) were obtained from TCI. N,N-dimethylformamide (DMF, 99%), N,N-diethylformamide (DEF, 99%), and dichloromethane (DCM, 99%) were obtained from VWR. *n*-Hexane (> 99%) and sodium chloride (NaCl, > 99.5%) were obtained from Merck Millipore. A Milli-Q unit (Millipore, USA) was used to supply deionized water.

Experimental Methods

Synthesis of ZrT-1-NH_2. ZrT-1-NH_2 was synthesized based on the previously reported method.[1] Zirconocene dichloride (0.3 g, 1.0 mmol) and 2-aminoterephthalic (0.1 g, 0.6 mmol) were added to DEF (10 mL) with deionised water (2 mL). The mixture was briefly sonicated and heated at 65 °C for at least 3 hours. Yellow cubic crystals formed on the vial walls. The products were washed with DMF and exchanged with DCM for two days.

Synthesis of Ti_4L_6-MOC. Ti_4L_6-MOC was synthesized based on the previously reported method.[2] Pamoic acid (0.038g, 0.098 mmol) was first dispersed thoroughly in 6 mL of *n*-propanol/DMF (v/v = 3:1) before titanium (IV) chloride (90 μL, 0.4 mmol) and 2 drops of ethylenediamine were added to give orange suspension. The suspension was heated at 100 °C

for at least 1 day until red crystals were obtained. The crystals were washed with hot *n*-propanol/DMF (3:1 v/v) until no orange residues were observed.

Preparation of Thin-Film Composite Membranes. The PA layer was prepared using the interfacial polymerization method on a PES UF substrate. The substrate was first mounted on a frame, and the PES side was exposed to 2 w/v% MPD in 3:2 acetone/water for 2 minutes. The MPD solution was then poured away. Excess MPD solution was removed by drying the coupon between two pieces of filter paper with a rubber roller. The coupon was then remounted on the frame and exposed to 0.15 w/v% TMC in *n*-hexane for 1 minute. The TMC solution was decanted, and the nascent membrane was washed with fresh *n*-hexane to quench further reactions. The membrane was dried for about 30 s before being briefly washed with running DI water and stored in 4 °C DI water overnight before use.

Preparation of Thin-Film Nanocomposite Membranes Containing MOCs. Ti_4L_6-MOC- and ZrT-1-NH_2-incorporated TFN membranes were prepared similarly. Previously, it has been found that it is necessary to completely dissolve the MOC in the aqueous solution, which requires adding a substantial amount of polar organic solvents such as acetone or methanol.[3, 4] Similarly, the dissolution of Ti_4L_6-MOC can be sped up by adding acetone. Therefore, the MOCs were processed in acetone/water (v/v = 3:2). Ti_4L_6-MOC or ZrT-1-NH_2 of various concentrations were added to the MPD solutions and applied to the PES UF substrates to deposit the cages on the surface of the substrate. TFN membranes are named as 0.0x-TFN-Ti (for membranes containing Ti_4L_6-MOC) and 0.0x-TFN-Zr (for membranes containing ZrT-1-NH_2); 0.0x is the weight percentage of MOCs in the MPD solution. The membranes were denoted as 0.02-TFN and so on, corresponding to the initial w/v% of MOC in MPD solution. For example, the 0.06-TFN-Ti membrane was fabricated by exposing the PES membrane to an MPD solution containing 3 mg of Ti_4L_6-MOC per 5 mL of MPD solution.

Membrane Separation Test. The water permeability and salt rejection of the TFC and ZrT-1-NH_2 TFN membranes were measured with a dead-end reverse osmosis filtration setup at room temperature. The feedwater near to membrane surface was stirred at 450 rpm to minimize concentration polarization. A membrane of an effective area of 1.77 cm^2 was compacted at 15.5 bars with 2000 ppm sodium chloride (NaCl) solution for 30 minutes until the permeate flux became stable. The membrane water flux (J_w) was calculated by normalizing the volume of permeate (V) by the effective surface area of membrane (A) in contact with feedwater and the collection duration (Δt):

$$J_w = \frac{V}{A \times \Delta t} \qquad \text{Eq. (1)}$$

The salt rejection is calculated by:

$$R = \left(1 - \frac{C_p}{C_f}\right) \times 100\% \qquad \text{Eq. (2)}$$

where C_p and C_f are conductivities of permeate and feed solutions, respectively, and were obtained from conductivity measurements.

Membrane Fouling Test. Dynamic membrane fouling was conducted with bovine serum albumin (BSA) as the model protein and dodecyltrimethyl ammonium bromide (DTAB) as the positively charged fouling model. Briefly, a membrane was first compacted with 2000 ppm NaCl solution at a transmembrane pressure of 16 bars for 30 min before recording the initial water flux. The feedwater was then changed to feed containing foulants. The concentrations of foulants are 200 ppm for BSA and 10 ppm for DTAB. NaCl (2000 ppm) was added to the foulant solution to check if any salt-permeating defects formed on the membrane during the test. Considering the effect of foulant retention, resistance by cake formation would be significant and pronounced in a more permeable membrane.[5-7] This would result in an underestimation of the antifouling capability. Therefore, we determined the fouling rate by tracing the membrane permeability as a function of the volume of permeates collected. The

foulant test was conducted until about 6 mL of permeate was collected for BSA and about 3mL of permeate for DTAB fouling due to the significant fouling that drastically reduced permeance. After fouling, the system was flushed with 300 mL of pure water. The membrane was further washed in pure water for 10 min with 1000 rpm stirring and 300 mL pure water flushing. During this process, loosely bound foulants were removed. The cleaned membrane was then tested with 2000 ppm NaCl feed to quantify the antifouling capabilities of the membrane by calculating the flux recovery ratio (FRR) and retention ratio (RR). FRR is given by f_c/f_i and RR is given by f_f/f_i, (f_i is the initial flux, f_f is the flux after fouling duration, and f_c is the water flux after membrane cleaning).

Static Membrane Fouling Test. To ensure the vitality of BSA, the BSA-FITC was dissolved in phosphate buffer solution at pH 6.4. Considering the common environments of working RO membranes, membrane fouling was conducted in dark environments. Bovine serum albumin-fluorescein isothiocyanate conjugate (BSA-FITC, 0.5 mg/mL) was dissolved in phosphate buffer saline (PBS) containing 0.137 M NaCl, 2.7 mM KCl, 10 mM Na_2HPO_4, and 1.8 mM KH_2PO_4, and adjusted to pH 6.4 with 0.5 M NaOH and 0.5 M HCl. BSA-FITC solution was stored at 4 °C until use. Wet membranes were dried with filter paper before being fixed onto a frame that exposed only the PA side. The membranes were exposed to BSA-FITC solution (0.5 mL) for 2.5 h in the dark. Fouled membranes were then washed thoroughly with flowing deionized water to remove loosely attached BSA-FTIC and air-dried for subsequent observation under a fluorescence microscope using the FITC channel. At this emission wavelength, the green BSA-FITC signal is undisturbed by the blue fluorescence of ZrT-1-NH_2. For consistency, the center of the membranes was compared.

General Characterizations. Characterizations of MOCs were conducted directly without further modification, while membranes may be first treated with DCM to isolate the polyamide layers for characterizations. Surface and cross-section morphology of membranes was

observed with field–emission scanning electron microscopy (FE–SEM) and atomic force microscopy (AFM). FE-SEM was conducted on a JEOL JSM–7610F scanning electron microscope. Each sample was treated with platinum sputtering before observation. AFM was conducted on Bruker Dimension ICON with Nanoscope V controller using tapping mode. The AFM data were processed with Nanoscope 9.7 and NanoScope Analysis 2.0. The elemental compositions in the membranes were probed with Fourier transform infrared spectrum (FT-IR) and energy dispersive X-ray spectrometry (XPS). FT-IR was measured using an attenuated total internal reflectance Fourier transform infrared spectrometer (ATR-FTIR, Alfa, Bruker), collecting absorption spectra from 400 to 4000 cm^{-1} and averaged over 32 scans. XPS was analyzed using X-ray photoelectron spectroscopy (XPS, AXIS Ultra DLD, Kratos X-ray photoelectron spectrometer, monochromatic Al Kα radiation (1486.71 eV) at 15 kV). Ultraviolet-visible spectrometry (UV–Vis) and confocal laser fluorescence microscopy (CLM) were conducted to identify MOCs in membranes. Liquid UV-Vis spectra were collected on a Shimadzu UV–3600 spectrometer. The solid-state UV-Vis spectra were obtained with a Shimadzu UV-2450 spectrophotometer using $BaSO_4$ as the standard. CLM was conducted with a Nikon A1plus camera and Ti microscope. The polyamide layers of the membranes were viewed under UV (402 nm) or FITC (488 nm) laser channels through an Apo 20x λS DIC N2 objective lens. The setting of both channels was kept the same to reflect the actual intensities. Confocal images were acquired with the NIS-Elements C package. Fluorescence microscopy images were acquired with a Nikon Ti-U fluorescence microscope at 50% intensity and NIS-Elements D. The membrane surface charge was analyzed with SurPASS electrokinetic analyzer (Anton Paar GmbH) with 0.01 M NaCl. The zetapotential of MOCs was analyzed with Malvern Zetasizer (Malvern Instruments, UK). Thermogravimetric analyses (TGA) were conducted using a Shimadzu DTG-60AH with an airflow rate of 50 mL/min. The samples were heated from 25 °C to 700 °C at a rate of 10 °C/min. Nitrogen gas sorption tests were conducted at 77

K using the freshly synthesized Ti_4L_6-MOC activated at 80 °C under vacuum for 8 h on a Quantachrome Autosorb iQ3 surface area and pore size analyzer. Powder X-ray diffraction patterns were obtained on a Rigaku MiniFlex 600 X-ray powder diffractometer equipped with a Cu sealed tube (λ = 1.5418 Å) operating at 40 kV, 15 mA, with a scan rate of 2 deg min^{-1}. Contact angle measurements were conducted on a telescopic goniometer (Rame–Hart, Model 100–00– (230)).

Pre-Treatment of Membrane Substrates. Dry PES UF substrate was cut into suitable sized coupons and soaked in isopropyl alcohol (IPA) for 1 h before soaking and washing thoroughly with aliquots of cold deionized water until IPA was mostly removed. The IPA-treated coupons were then stored in cold deionized water at 4 °C overnight before exchanging with fresh cold deionized water. This was repeated one more time to ensure that most IPA had been removed. The PES UF coupons were stored in cold deionized water at 4 °C until use.

Isolation of Polyamide (PA) Layer for Characterizations. The fresh membrane was dried under a vacuum at 55 °C overnight. The dried membrane was soaked in dichloromethane until the PA layer detached from the substrate. The PA layer was collected and washed with fresh aliquots of dichloromethane until no white residues were observed. The samples were placed at 25 °C under vacuum for at least 1 h to remove residual dichloromethane.

Thermogravimetric Analyses (TGA) of MOCs and Membranes. TGA tests under an oxidative atmosphere (e.g., air) can burn away the organic portion of the membrane and MOCs, leaving zirconium oxide or titanium oxide, depending on the type of MOCs. This will estimate the loading of MOCs in the PA layer. The samples were heated from room temperature to 700 °C in air at a heating rate of 10 °C/min. The content of MOCs was calculated using the following equation with ZrT-1-NH_2 as an example:

$$Zr\ \text{wt\%} = \frac{(\frac{m_r}{m_t})_{TFN} - (\frac{m_r}{m_t})_{TFC}}{(\frac{m_r}{m_t})_{ZrT-1-NH2}} \times 100\% \qquad \text{Eq. (3)}$$

where m_t and m_r refer to the total mass of sample loaded initially and the residual mass after burning, respectively.

Gas Sorption Tests. Freshly synthesized Ti_4L_6-MOC in 1-propanol/dimethylformamide (v/v = 3:1) was exchanged with DCM over two days. Excess DCM was poured away, and the sample was activated at 80 °C under a vacuum for 8 h.

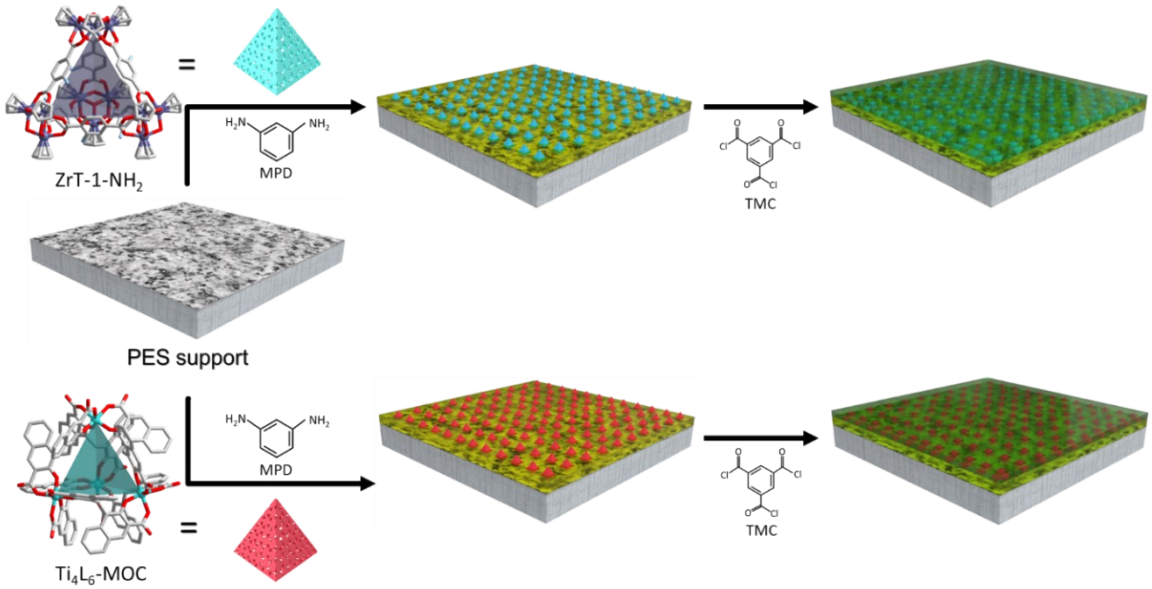

Supplementary Figure S1. Scheme of TFN-Zr and TFN-Ti membrane fabrication. Color code of ZrT-1-NH_2 and Ti_4L_6-MOC: purple: Zr, green: Ti, red: O, light blue: N, grey: C, purple polyhedral: space within ZrT-1-NH_2, green polyhedra: space within Ti_4L_6-MOC.

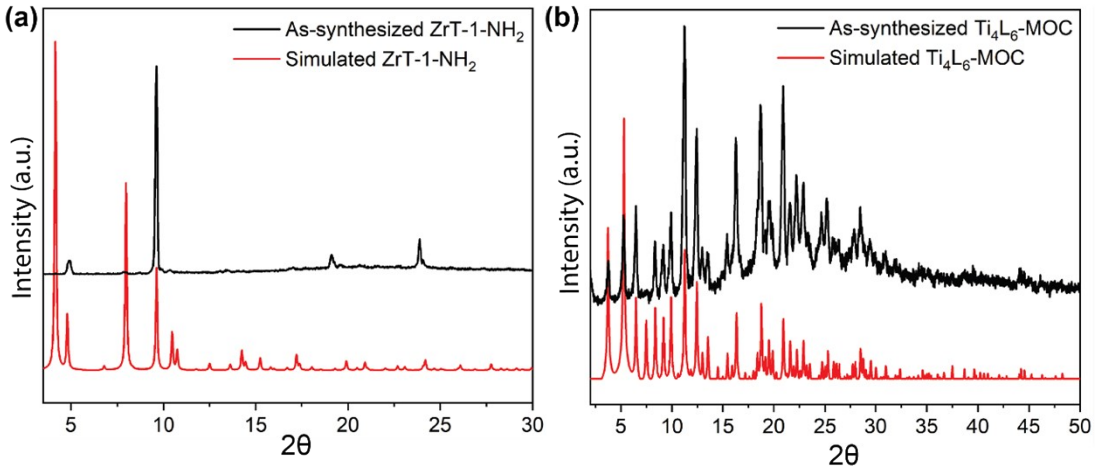

Supplementary Figure S2. PXRD spectra of ZrT-1-NH_2 (a) and Ti_4L_6-MOC (b).

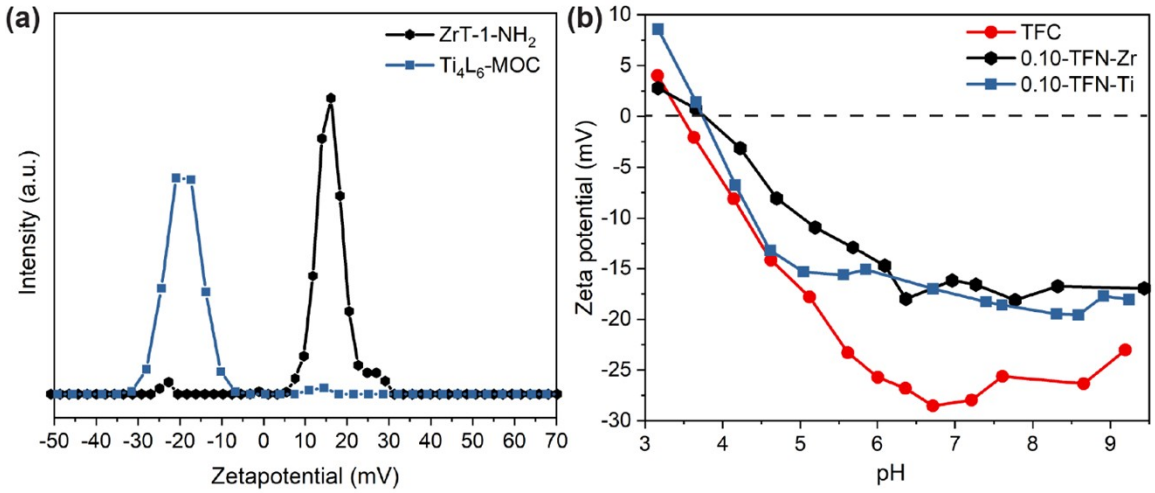

Supplementary Figure S3. (a) Zeta potential of Ti_4L_6-MOC and ZrT-1-NH_2 in acetone/water (3:2 v/v). (b) Zeta potential of TFC, 0.10-TFN-Zr, and 0.10-TFN-Ti under various pH values in 0.01 M NaCl solution.

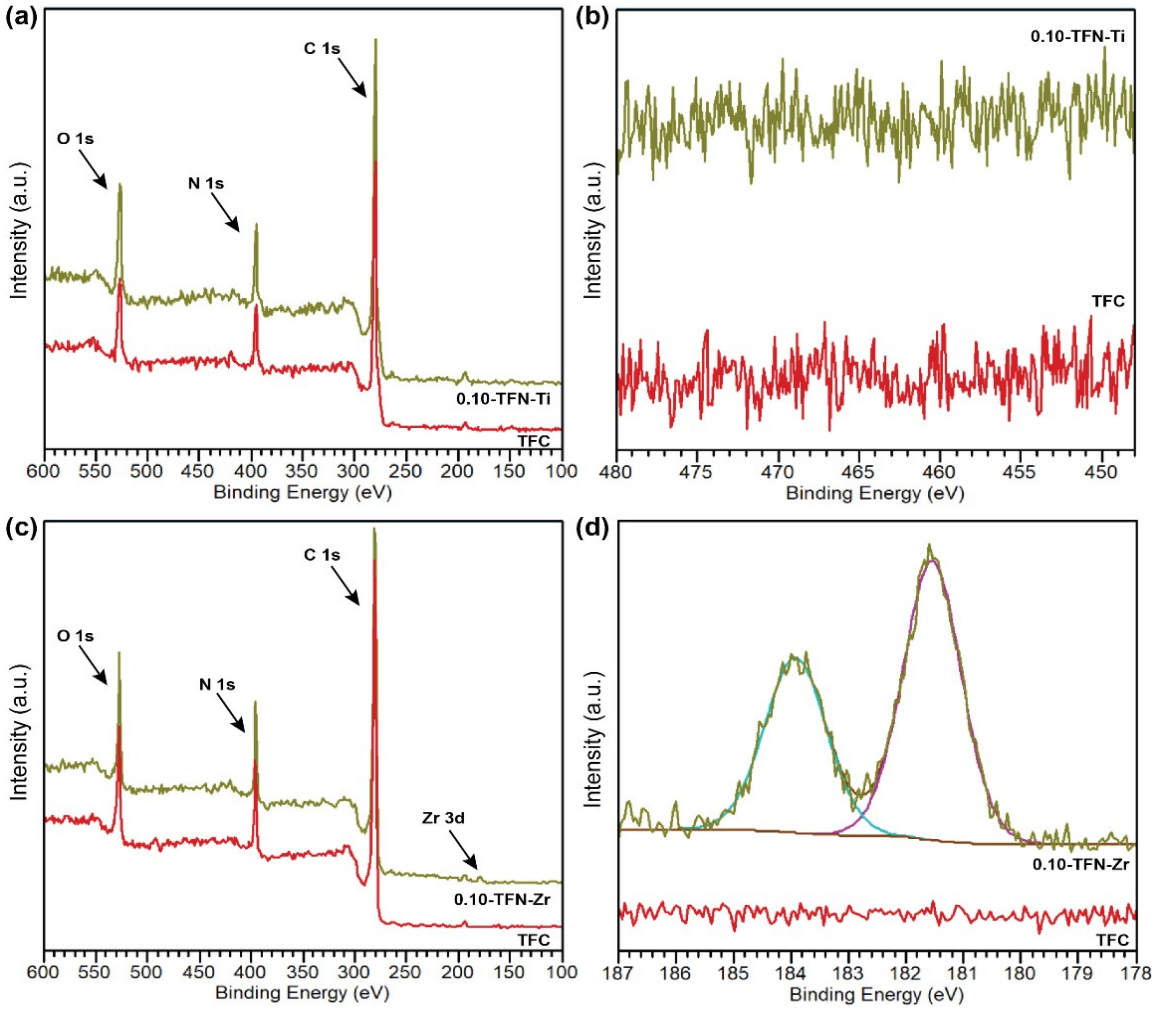

Supplementary Figure S4. XPS spectra of survey (a) and Ti 2p region (b) of TFC and 0.10-TFN-Ti membranes, and survey (c) and Zr 3d region (d) of TFC and 0.10-TFN-Zr membranes.

Note: TFN-Zr membranes with two peaks located at 181.5 eV and 184 eV, corresponding to Zr $3d_{5/2}$ and Zr $3d_{3/2}$, respectively.[8]

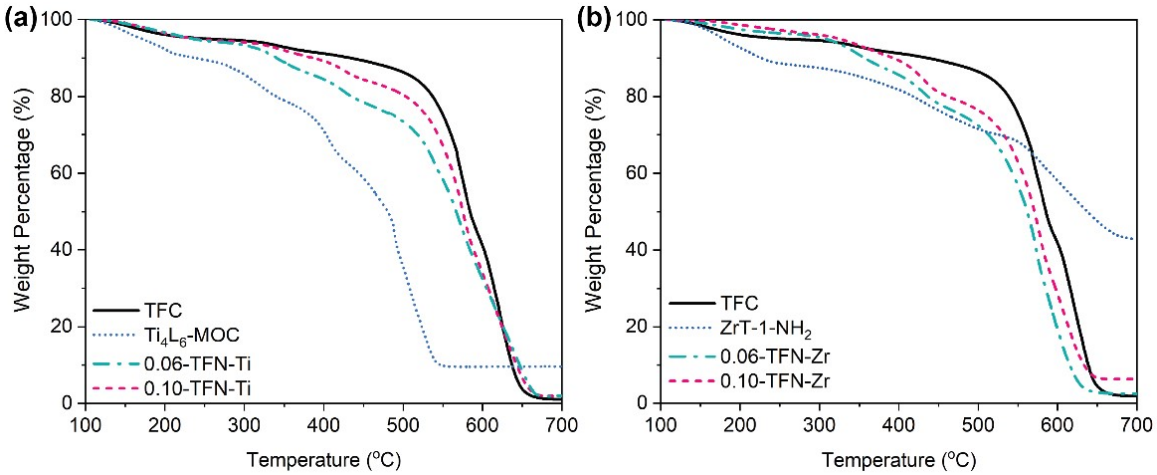

Supplementary Figure S5. TGA curves of TFN-Ti (a) and TFN-Zr (b) membranes.

Note: During TGA, the PA layers of TFN-Zr membranes were burned in air until 700 °C, and their residual zirconium oxide masses represent the amount of Zr originally contained in the PA layer. After correcting with the residual mass of pure ZrT-1-NH_2 powder, 0.06-TFN-Zr and 0.10-TFN-Zr contain 2.19 wt% and 9.96 wt%, respectively. It is apparent that the higher initial ZrT-1-NH_2 loading results in membrane with higher ZrT-1-NH_2 content. The content of ZrT-1-NH_2 in 0.10-TFN-Zr is even higher than the theoretical concentration of 4.76 wt%. This may be due to the deposition of heavier large ZrT-1-NH_2 aggregates on the membrane during fabrication. Therefore, although the reason for the constant Zr content on the membrane surface is not clearly known, it is possible, however, that the excess MOC is deposited deeper in the membrane. This saturation may have an adverse effect on the membrane performance where the formation of larger cage aggregates either form an unfavorable interface with the PA[9] or increase mass transport resistance.[10] This decrease in permeability due to higher cage loading was also observed in membranes containing other MOCs and POCs.[11]

On the other hand, 0.06-TFN-Ti and 0.10-TFN-Ti membranes contain 1.87 wt% and 1.82 wt% of Ti_4L_6-MOC, respectively, which are lower than the TFN-Zr. This corroborates that crosslinking of MOC to the polymeric matrices enhances MOC loading. The presence of TiO_2 in the TGA residue confirms that Ti_4L_6-MOC is present inside the polyamide layer, perhaps deeper into the polyamide matrix than on the surface since XPS was unable to detect its presence.

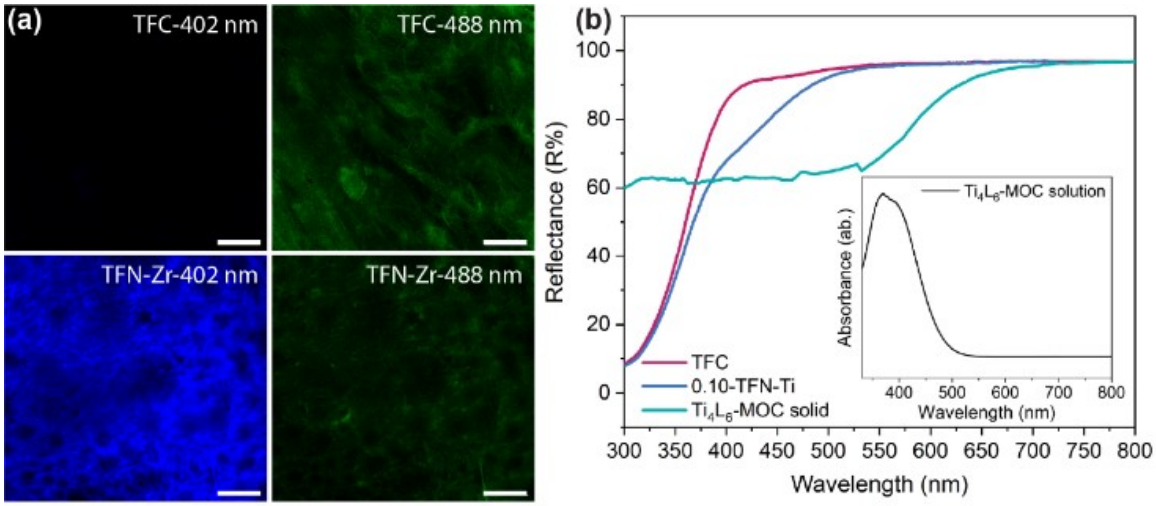

Supplementary Fig. S6. (a) Confocal laser spectroscopy of TFC and 0.10-TFN-Zr membrane at UV (Ex. 402 nm) and FITC (Ex. 488 nm) regions. The scale bar represents 100 µm. (b) UV-vis spectrum of solid Ti_4L_6-MOC, TFC, 0.10-TFN-Ti membrane and Ti_4L_6-MOC solution (insert).

Note: ZrT-1-NH_2 emits blue fluorescence under ultraviolet radiation when fully dissolved.[3] Therefore, the presence of blue fluorescence in the TFN-Zr membrane is a key indicator of well-dispersed ZrT-1-NH_2 in the PA layer. The intensity of the laser was set to be the same for both TFC and TFN-Zr. The difference between TFC-488 nm and TFN-Zr-488 nm is probably due to the lesser MPD-TMC linkage that gave weaker green fluorescence at 488 nm.

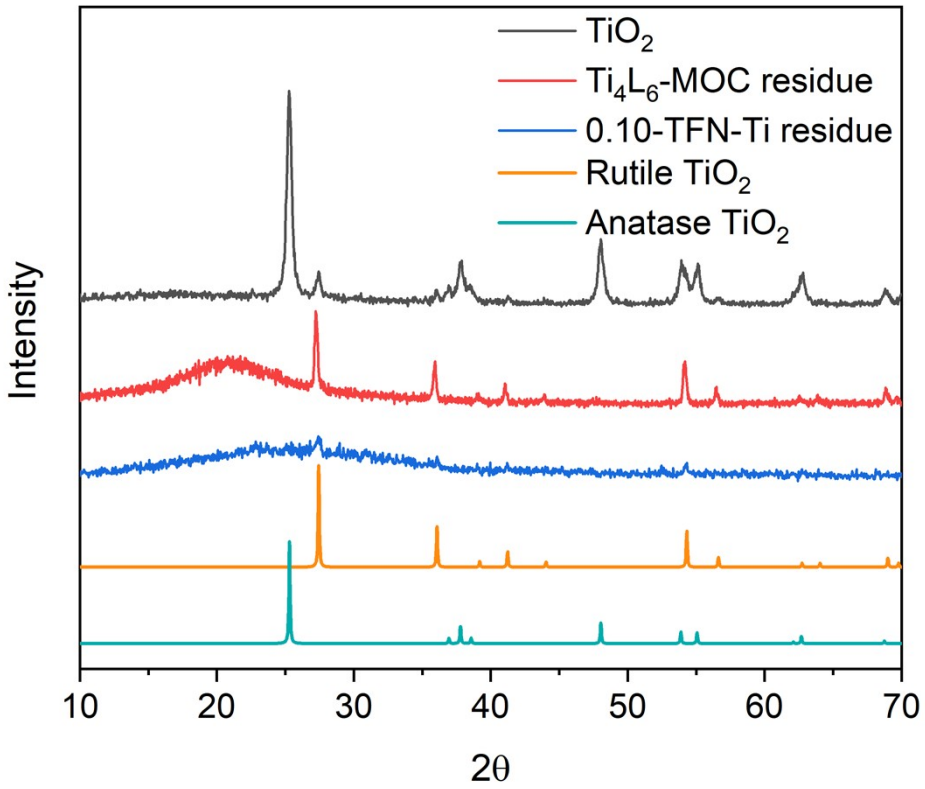

Supplementary Figure S7. PXRD patterns of the residual TiO_2 from TGA analysis. The white titanium oxide residue obtained from burning Ti_4L_6-MOC dispersed in the TFN-Ti had very weak crystallinity, with only peaks at 27.4° (110) and 54.3° (211) barely distinguishable but still matched to the patterns of commercial TiO_2 and residues found from Ti_4L_6-MOC crystals directly burned in air during TGA. The weak and amorphous peaks indicate that the residual TiO_2 exists as nanoparticles as compared to the micropowder residues,[12] which suggests that Ti_4L_6-MOC was well-dispersed inside the PA layer.

Note: TiO_2 (Aeroxide, P25) is a mixture of rutile[13] and anatase[14] phases. The Ti_4L_6-MOC and 0.10-TFN-Ti membrane TGA residues essentially display the rutile phase due to the high temperature of TGA that induced the transformation of anatase to the more stable rutile phase.[15]

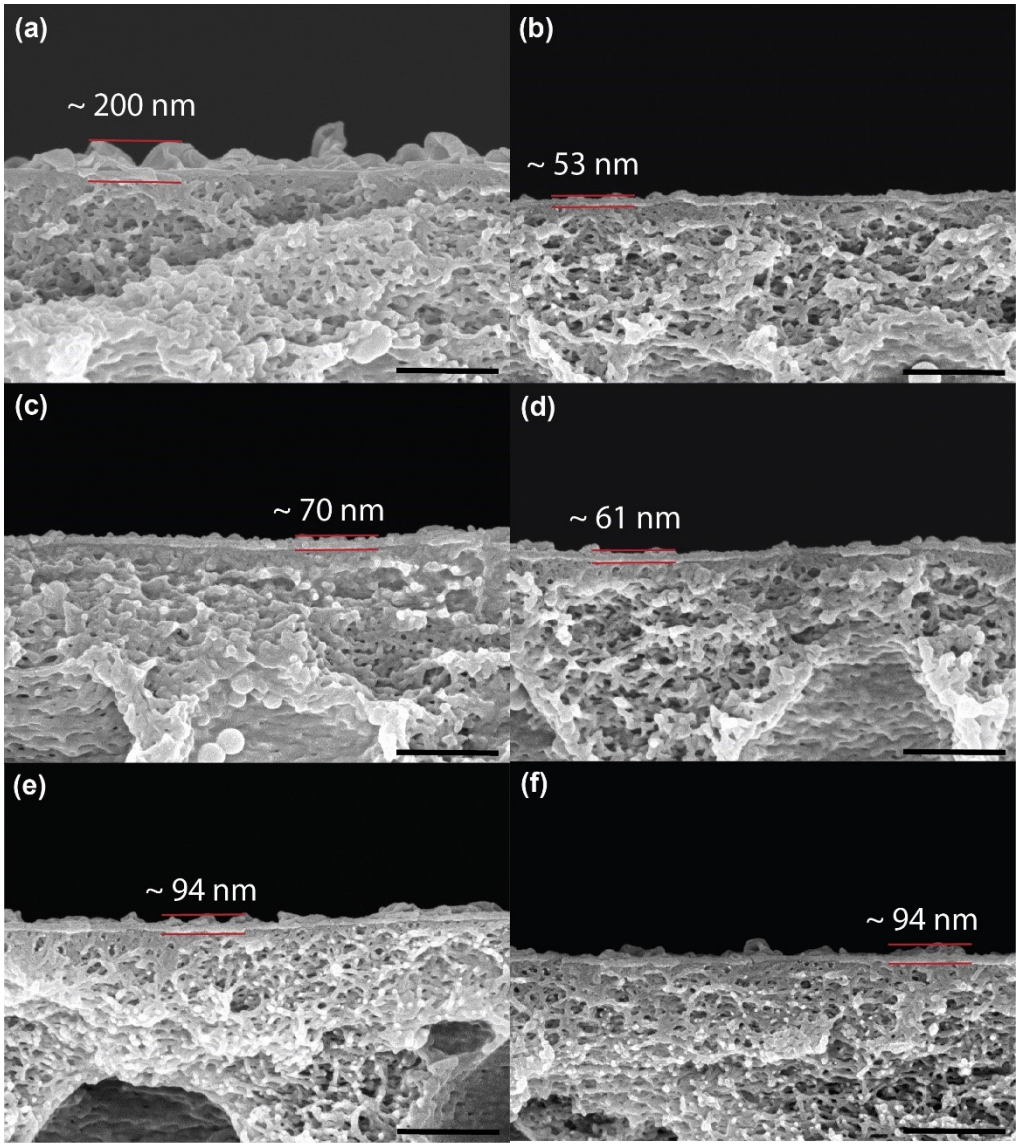

Supplementary Fig. S8. Cross-sectional FESEM image of (a) TFC, (b) 0.02-TFN-Zr, (c) 0.04-TFN-Zr, (d) 0.06-TFN-Zr, (e) 0.08-TFN-Zr, (f) 0.10-TFN-Zr. The scale bars represent 500 nm.

Note: TFC membrane has a relatively thick layer of polyamide membrane consisting of large leaflets. With the addition of a minute amount of ZrT-1-NH_2, the polyamide layer became thin, and large folds were absent. The thickening of the membrane beyond 0.04-TFN-Zr may have resulted in the lower membrane permeability.

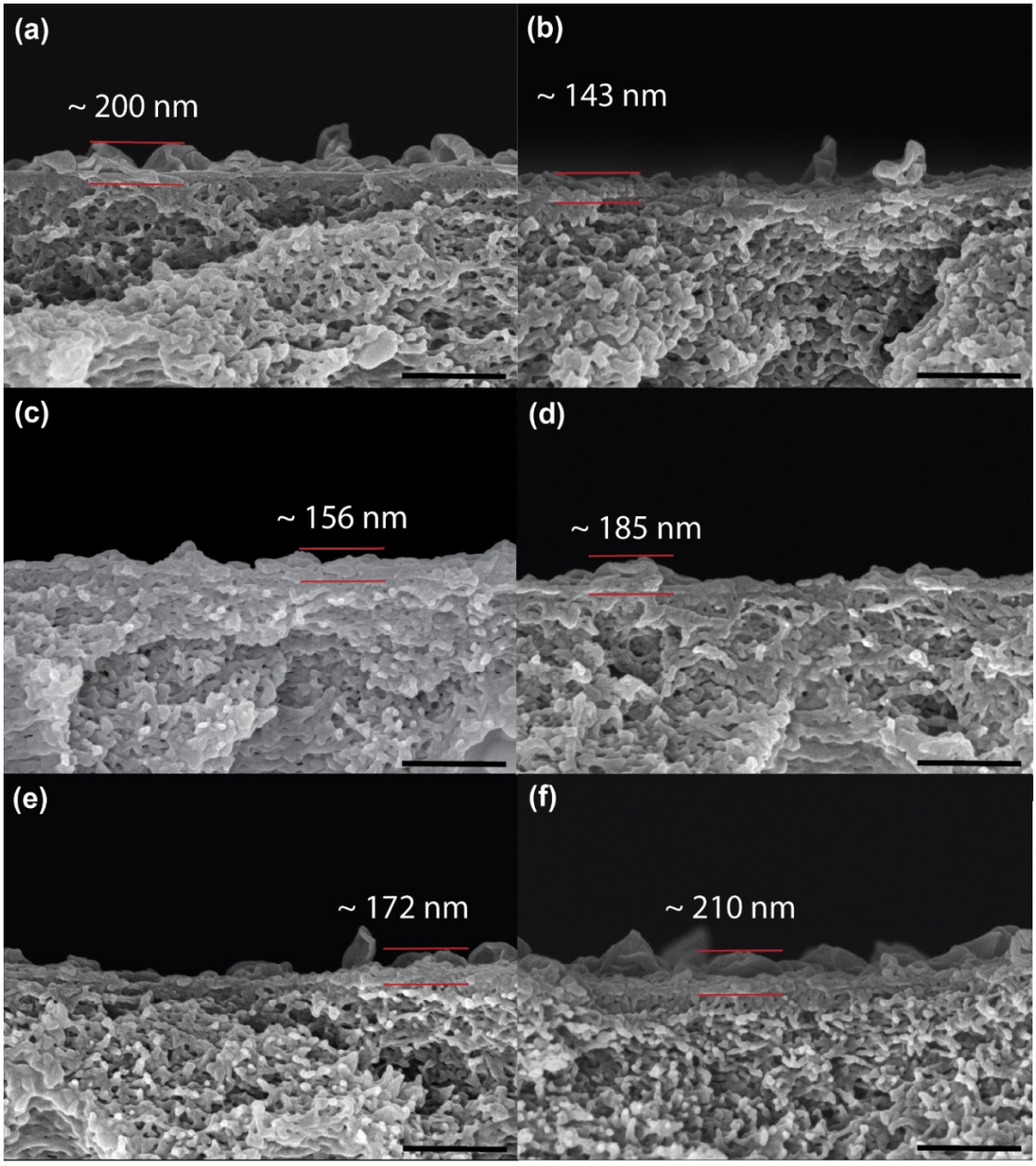

Supplementary Fig. S9. Cross-sectional FESEM image of (a) TFC, (b) 0.02-TFN-Ti, (c) 0.04-TFN-Ti, (d) 0.06-TFN-Ti, (e) 0.08-TFN-Ti, (f) 0.10-TFN-Ti. The scale bars represent 500 nm.

Note: The distinct leaflets of TFC polyamide layer disappeared when Ti_4L_6-MOC was added. Compared to TFN-Zr, TFN-Ti membranes are relatively thick but flatter compared to TFC due to the collapse of the leaflets. As the concentration of Ti_4L_6-MOC during membrane fabrication increases, large folds are again seen in higher concentration membranes such as 0.08-TFN-Ti and 0.10-TFN-Ti.

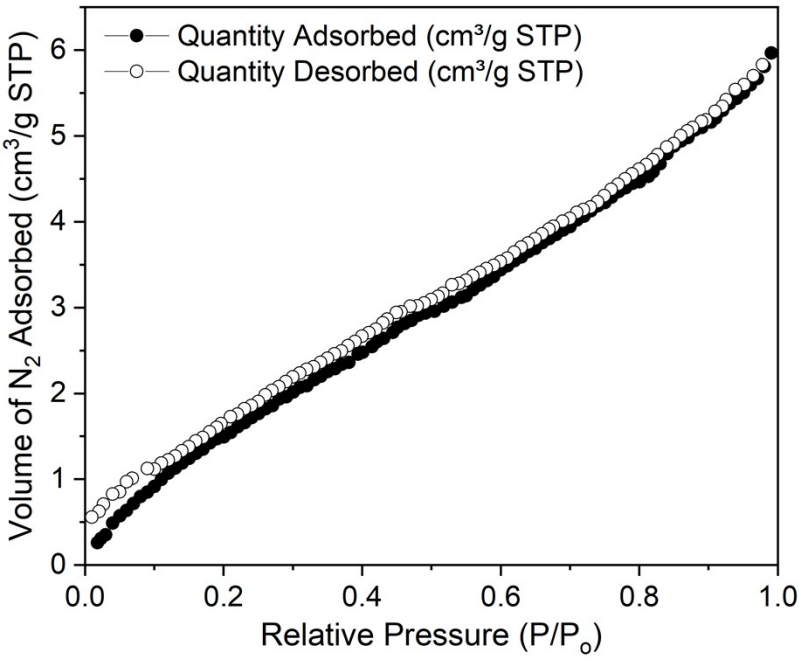

Supplementary Fig. S10. N_2 sorption on Ti_4L_6-MOC at 77 K.

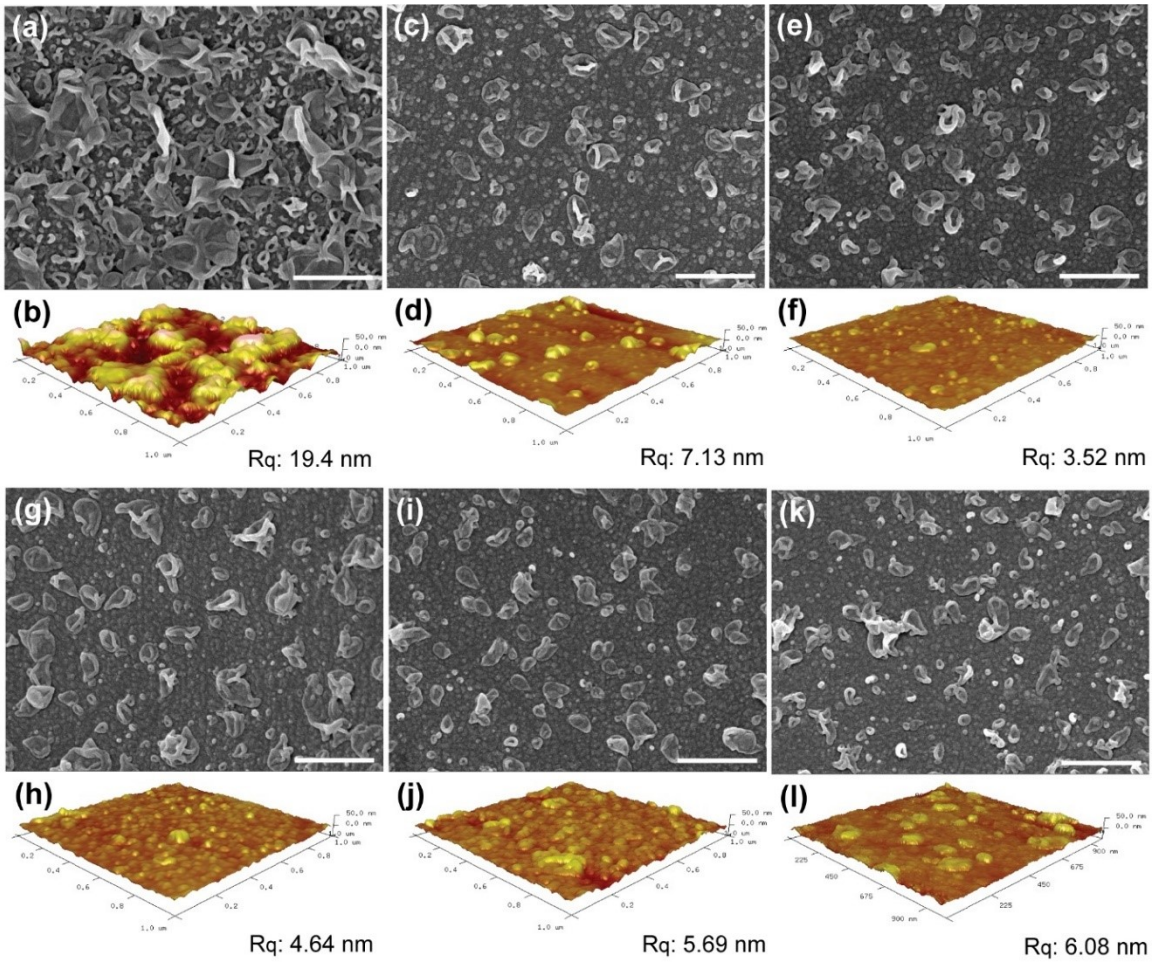

Supplementary Fig. S11. Surface morphologies of TFN-Zr membranes. SEM and AFM images of TFC (a, b), 0.02-TFN-Zr (c, d), 0.04-TFN-Zr (e, f), 0.06-TFN-Zr (g, h), 0.08-TFN-Zr (i, j), 0.10-TFN-Zr (k, l). The scale bars represent 500 nm.

Note: With the addition of ZrT-1-NH_2 into the polyamide layer, the selective layer morphology changed. The heavy ridges and leaflets characteristic of the TFC membrane was replaced by nodules and miniature leaflets when a minute amount of ZrT-1-NH_2 (0.02-TFN-Zr) was added, which resulted in a much smoother membrane surface. Further increase in the concentration during polyamide fabrication did not significantly affect the membrane surface morphology. This suggests that a very low concentration is sufficient to affect the polyamide morphology by participating in the polymeric matrix. Saturation is quickly reached such that higher concentration will no longer affect the membrane morphology.

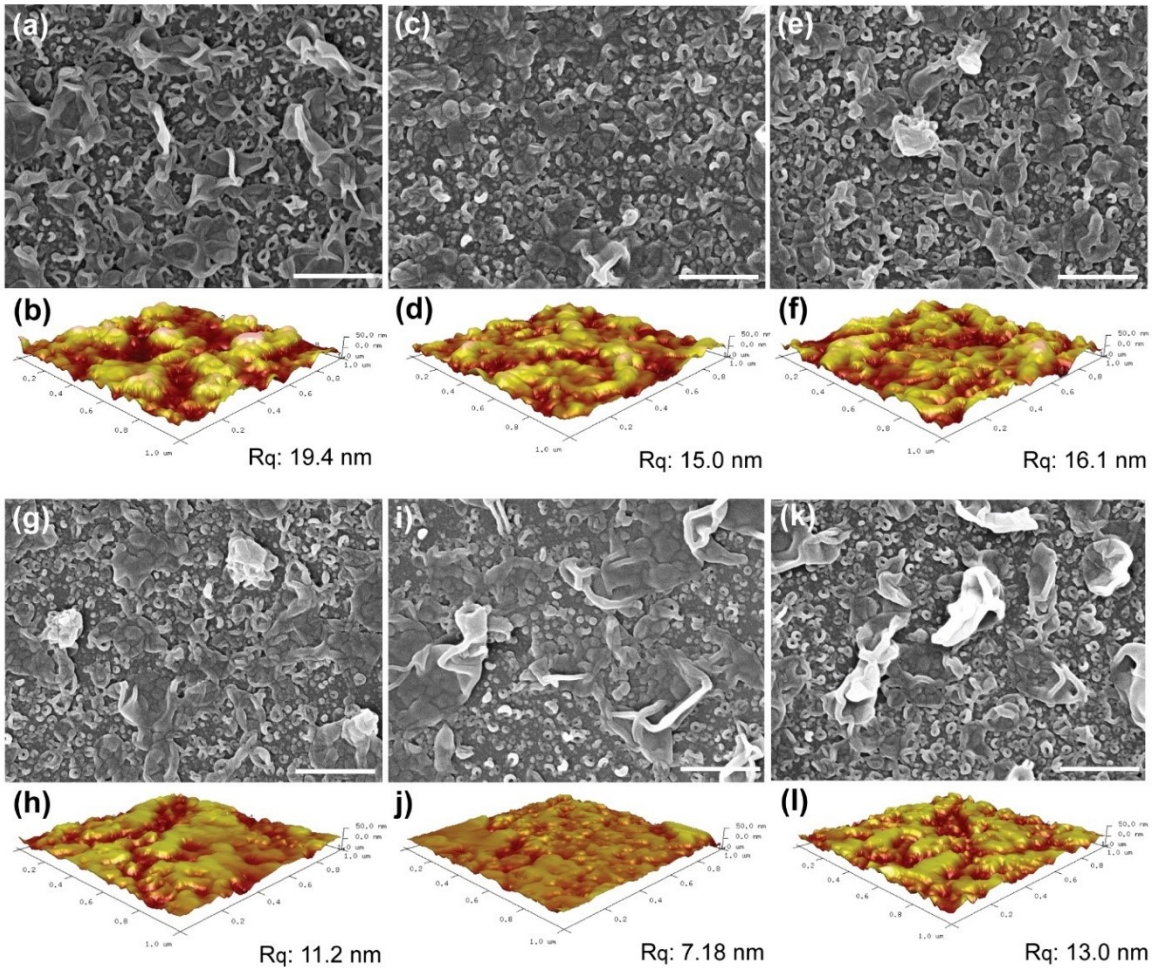

Supplementary Fig. S12. Surface morphologies of TFN-Ti membranes. SEM and AFM images of TFC (a, b), 0.02-TFN-Ti (c, d), 0.04-TFN-Ti (e, f), 0.06-TFN-Ti (g, h), 0.08-TFN-Ti (i, j), 0.10-TFN-Ti (k, l). The scale bars represent 500 nm.

Note: Unlike TFN-Zr membranes, the heavy ridges and leaflets persist in TFN-Ti membranes, but the leaflets seem to collapse on top of the ridges to form smooth areas. Higher concentrations of Ti_4L_6-MOC encouraged the formation of larger leaflets. The leaflets on 0.10-TFN-Ti were large enough to form thick folds that introduced more surface roughness.

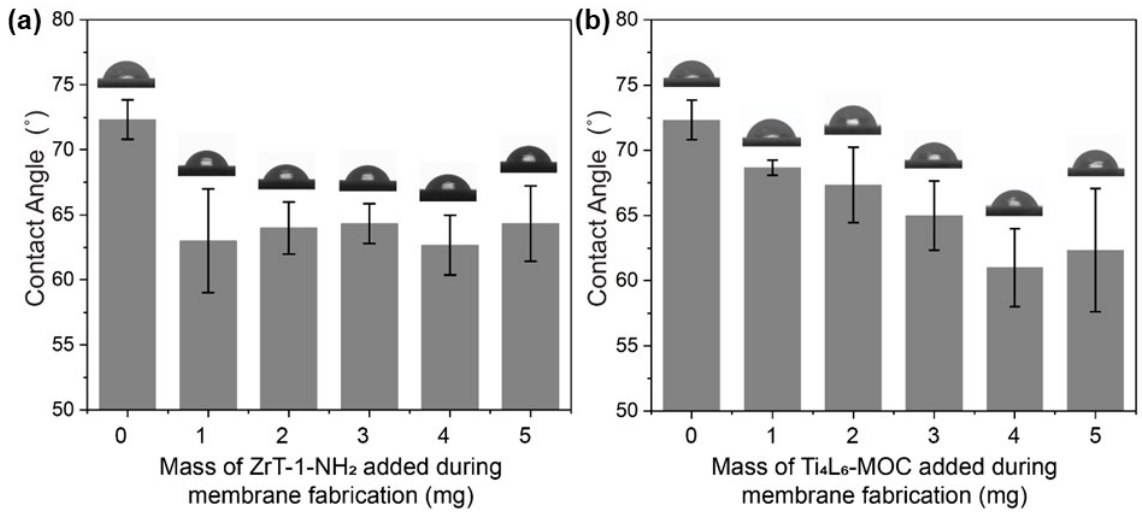

Supplementary Fig. S13. Contact angles of TFN-Zr (a) and TFN-Ti (b) membranes.

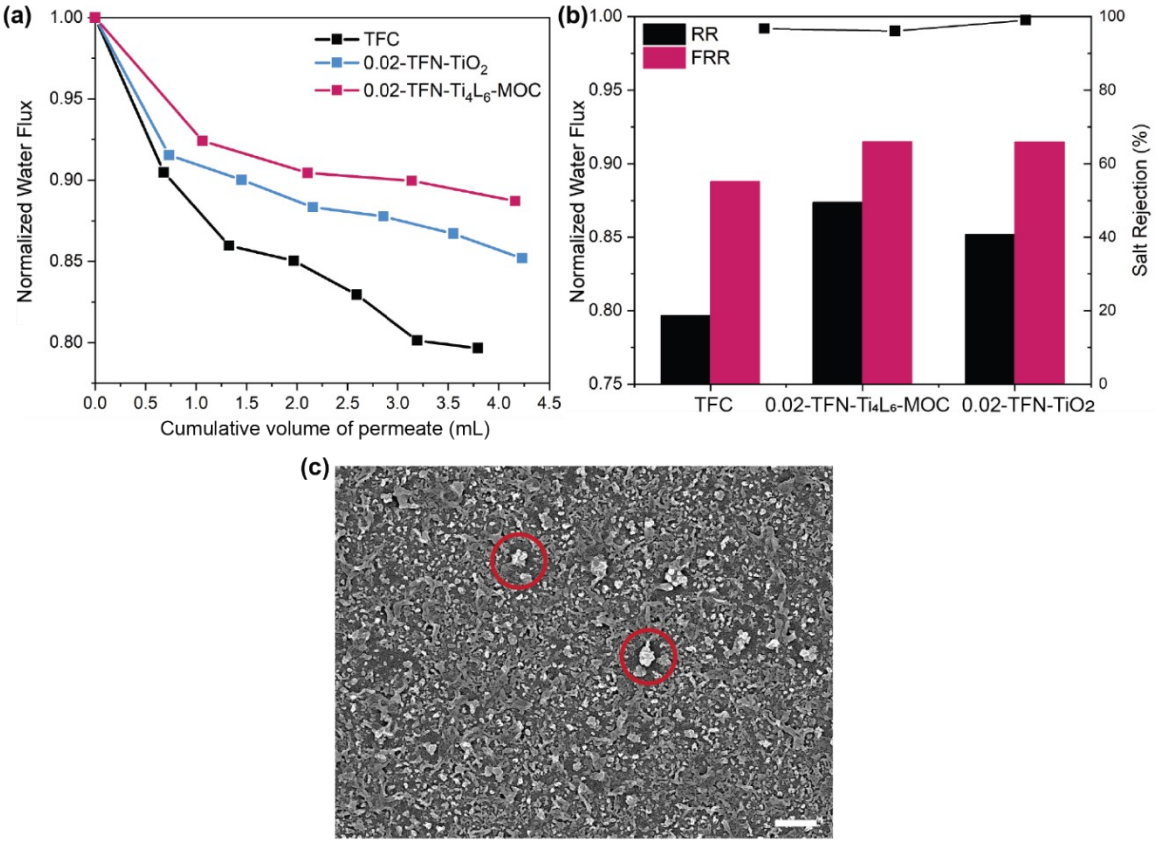

Supplementary Fig. S14. Antifouling study of TiO_2 compared to Ti_4L_6-MOC. (a) Dynamic BSA fouling of TFC, 0.02-TFN-Ti_4L_6-MOC, and 0.02-TFN-TiO_2. (b) Retention ratio (RR) and flux recovery ratio (FRR) of TFC, 0.02-TFN-Ti_4L_6-MOC, and 0.02-TFN-TiO_2 after BSA fouling and washing with DI water. (c) FESEM image of 0.02-TFN-TiO_2 with aggregates of TiO_2 circled in red. The scale bar represents 1 μm.

Note: Due to the stability of the MOCs, there should not be free metal ions in the membrane system. Assuming the Ti_4L_6-MOC dissociates in water or contains free metal ions, the $TiCl_4$ will react with water to form TiO_2. Hence, we compared Ti_4L_6-MOC with TiO_2. A dynamic BSA fouling test was conducted for membranes containing Ti_4L_6-MOC (0.02-TFN-Ti_4L_6-MOC) and TiO_2 (0.02-TFN-TiO_2). Within the testing period, the presence of TiO_2 and Ti_4L_6-MOC offered better antifouling capability. 0.02-TFN-Ti_4L_6-MOC appeared to foul less compared to 0.02-TFN-TiO_2. This may be attributed to the presence of Ti^{3+} in Ti_4L_6-MOC. Therefore, the entire Ti_4L_6-MOC structure, instead of its metal ions, contributed to the enhancement of the membrane's antifouling property. The 0.02-TFN-TiO_2 membrane retained the characteristic ridges and leaflets of TFC with some large TiO_2 aggregates dispersed on the membrane surface. Hence, membrane hydrophilicity may play a greater role than membrane morphology in the antifouling capability of 0.02-TFN-TiO_2 membrane.

Table S1. The effect of acetone on membrane performance.

Membrane	Water Flux (LMH)	Salt Rejection (%)
TFC	6.98 (± 0.37)	95.22 (± 0.73)
TFC-without acetone	14.88 (± 0.33)	95.74 (± 0.13)
0.04-TFN-Zr	24.32 (± 0.43)	96.49 (± 0.81)

Membranes tested at 15.5 bar, 2000 ppm NaCl condition. All data is an average of replicates of three.

Note: Acetone adversely affects the membrane performance, specifically the membrane water flux. However, acetone is currently required for the dissolution and incorporation of ZrT-1-NH_2 in the polyamide layer. The benefit of selective transport of water through ZrT-1-NH_2 justifies the addition of acetone.

Table S2. XPS atomic percentage of TFN-Zr membranes.

Sample	C (%)	O (%)	N (%)	Zr (%)	O/N
TFC	78.3 (± 2.2)	10.4 (± 1.8)	11.3 (± 0.65)	-	0.935 (± 0.163)
0.02-TFN-Zr	78.3 (± 1.5)	10.4 (±1.4)	11.1 (± 0.60)	0.233 (± 0.043)	0.976 (± 0.155)
0.04-TFN-Zr	77.6 (± 0.74)	10.4 (± 0.76)	11.8 (± 0.77)	0.223 (± 0.049)	0.916 (± 0.086)
0.06-TFN-Zr	78.2 (± 0.75)	9.99 (± 1.1)	11.6 (± 0.82)	0.225 (± 0.029)	0.908 (± 0.140)
0.08-TFN-Zr	78.6 (± 1.3)	9.36 (± 0.88)	11.8 (± 0.80)	0.203 (± 0.050)	0.847 (± 0.145)
0.10-TFN-Zr	79.0 (± 0.94)	9.59 (± 0.74)	11.2 (± 1.3)	0.225 (± 0.044)	0.789 (± 0.225)

Note: The atomic percentage of surface Zr on various TFN-Zr membranes remained relatively constant irrespective of the initial loading concentration and the total ZrT-1-NH_2 content in the PA layer, as determined by TGA.

Table S3. XPS atomic percentage of TFN-Ti membranes.

Sample	C (%)	O (%)	N (%)	Ti (%)	O/N
TFC	80.37	9.45	10.19	-	0.927
0.02-TFN-Ti	78.56	11.45	11.99	-	0.955
0.04-TFN-Ti	77.8	10.49	11.72	-	0.895
0.06-TFN-Ti	80.09	9.37	10.54	-	0.889
0.08-TFN-Ti	76.57	11.07	12.36	-	0.896
0.10-TFN-Ti	78.54	10.24	11.22	-	0.913

Note: The presence of Ti was not detected.

Reference

1. G. Liu, Z. Yang, M. Zhou, Y. Wang, D. Yuan and D. Zhao, *Chem. Commun.*, 2021, **57**, 6276–6279.
2. Y.-P. He, L.-B. Yuan, G.-H. Chen, Q.-P. Lin, F. Wang, L. Zhang and J. Zhang, *J. Am. Chem. Soc.*, 2017, **139**, 16845–16851.
3. G. Liu, X. Zhang, Y. D. Yuan, H. Yuan, N. Li, Y. Ying, S. B. Peh, Y. Wang, Y. Cheng, Y. Cai, Z. Gu, H. Cai and D. Zhao, *ACS Mater. Lett.*, 2021, **3**, 268–274.
4. Z. Yang, G. Liu, Y. D. Yuan, S. B. Peh, Y. Ying, W. Fan, X. Yu, H. Yang, Z. Wu and D. Zhao, *J. Membr. Sci.*, 2021, 119564.
5. K. Listiarini, W. Chun, D. D. Sun and J. O. Leckie, *J. Membr. Sci.*, 2009, **344**, 244–251.
6. A. S. Kim and E. M. V. Hoek, *Environ. Eng. Sci.*, 2002, **19**, 373–386.
7. Y. Bessiere, N. Abidine and P. Bacchin, *J. Membr. Sci.*, 2005, **264**, 37–47.
8. M. Sun, Q.-Q. Wang, C. Qin, C.-Y. Sun, X.-L. Wang and Z.-M. Su, *Chem. Eur. J.*, 2019, **25**, 2824–2830.
9. R. Han and P. Wu, *ACS Appl. Mater. Interfaces*, 2018, **10**, 18351–18358.
10. L. Liu, X. Xie, S. Qi, R. Li, X. Zhang, X. Song and C. Gao, *J. Membr. Sci.*, 2019, **580**, 101–109.
11. G. Zhu, F. Zhang, M. P. Rivera, X. Hu, G. Zhang, C. W. Jones and R. P. Lively, *Angew. Chem. Int. Ed.*, 2018, **58**, 2638–2643.
12. X. Cao, J. Ma, X. Shi and Z. Ren, *Appl. Surf. Sci.*, 2006, **253**, 2003–2010.
13. P. Villar, PAULING FILE in: Inorganic Solid Phases. TiO2 rutile (TiO2 rut) Crystal Structure. *SpringerMaterials (online database)*, Springer, Heidelberg (ed.), 2016.
14. C. J. Howard, T. M. Sabine and F. Dickson, *Acta Crystallogra. B*, 1991, **47**, 462–468.
15. D. A. H. Hanaor and C. C. Sorrell, *J. Mater. Sci.*, 2011, **46**, 855–874.